

Article

A Wideband High-Voltage Power Amplifier Post-Linearizer for Medical Ultrasound Transducers

Hojong Choi ¹, Changan Yoon ^{2,*} and Jung-Yeol Yeom ^{3,*}

¹ Department of Medical IT Convergence Engineering, Kumoh National Institute of Technology, Gumi 39253, Korea; hojongch@kumoh.ac.kr

² Department of Biomedical Engineering, Inje University, Gimhae 50834, Korea

³ School of Biomedical Engineering, Korea University, Seoul 02841, Korea

* Correspondence: cyoon@inje.ac.kr (C.Y.); jungyeol@korea.ac.kr (J.-Y.Y.); Tel.: +82-55-320-3301 (C.Y.); +82-2-3290-5662 (J.-Y.Y.)

Academic Editor: Richard Y. Q. Fu

Received: 21 January 2017; Accepted: 23 March 2017; Published: 4 April 2017

Abstract: The medical ultrasound transducer is a principal component in ultrasound systems, as it significantly influences system performance. The high-voltage power amplifier (HVPA) is the key ultrasound transmitter component and interfaces with the medical ultrasound transducer. Therefore, the performance of the HVPA critically affects the echo signal quality of the ultrasound transducer. As they are inherently non-linear devices, harmonic distortion of echo signals generated by the ultrasound transducers would critically deteriorate the echo signal quality in ultrasound systems. The primary aim of this research is to integrate a novel post-linearizer into the HVPA to suppress harmonic distortion in medical ultrasound transducers. Moreover, this study is based on the assumption that linearizing the HVPA could reduce the harmonic distortion components of the echo signals. The developed HVPA with post-linearizer was tested in an ultrasound microscopy system in order to demonstrate the harmonic suppression capability on the echo signal generated by the ultrasound transducer. When 10 MHz, 5-cycle, 26 dB_m input power was sent to the HVPA with and without the post-linearizer circuits, the measured second-, third-, fourth- and fifth- harmonic distortions of a 10 MHz transducer with the post-linearizer (−13.11 dB, −10.81 dB, −16.33 dB, and −22.78 dB) were suppressed to a greater degree than those of the same transducer without the post-linearizer (−4.58 dB, −8.87 dB, −10.51 dB, and −15.31 dB).. Therefore, we conclude that the addition of the post-linearizer to the HVPA is a potentially useful electronic technique for improving echo signal quality in medical ultrasound transducers.

Keywords: post-linearizer; medical ultrasound transducer; high-voltage power amplifier

1. Introduction

Ultrasound systems have been used in various applications, such as nondestructive testing, medical imaging, acoustic tweezers, cellular stimulation and surface acoustic wave filters [1–5]. In ultrasound systems, the transmitters are one of the key components affecting the ultrasound transducer performance [6–8]. The high-voltage power amplifier (HVPA) is a critical ultrasound transmitter component that influences the generation of ultrasound waves by the transducer [9,10]. More specifically, adjacent channels in the miniaturized array transducer result in cross-intermodulation and signal harmonic distortions [11,12]. Therefore, the HVPA in medical ultrasound transmitters should yield low-harmonic distortions [13,14]. Harmonic imaging technique (HIT) in ultrasound systems is commonly used to enhance image contrast by using a relatively higher bandwidth of the received echo signals [15–17]. When applying the HIT, the transmitting signal produced from the HVPA should have low-harmonic components because the image is formed solely from the several harmonic components

generated by the target and these harmonic components should not interfere with the transmitting harmonic components of the HVPA [7]. The coded excitation method is generally utilized to increase the signal-to-noise ratio of echo signals. However, this method also requires low-harmonic signal distortion to prevent spectral overlap [18].

In wireless communication systems, power amplifier linearizing techniques have been widely used to eliminate the narrow-band channel selection of the operating data signal carrier frequency, and to reduce leakage signal from the transmitter [19,20]. A linear HVPA is also desirable in ultrasound systems because the multiple-order (second, third, and fourth) harmonic components of the echo waveform generated by the medical ultrasound transducer deteriorate the echo signal quality of ultrasound systems [7].

The harmonic distortion components in ultrasound applications are critical issues to address, because higher harmonic distortion components of the echo signals lower image resolution [21]. The non-linear ultrasound wave (ultrasound wave with high harmonic distortions) causes ultrasound wave distortion. As a result of the distorted ultrasound wave, image resolution of ultrasound instrumentation is degraded, and even the penetration depth into the medium is reduced [10]. In order to reduce the high-order harmonic distortion components, several methods using contrast agents or signal-processing techniques have been reported. The first method involves using a contrast agent in which the pulse-echo response capability is improved using insonification, thus reducing unwanted backscattered echo signals [22]. However, dynamic quantification of contrast agents is not possible with this method. The second method is to suppress harmonic signals by performing a series of signal-processing operations without using contrast agents [17], described as follows: (1) pulse-inversion is first applied to the ultrasound system followed by harmonic post-processing [23]. However, this method critically reduces the frame rate of the ultrasound system. (2) Source pre-biasing can be used to shift the phase between the fundamental pulse and leakage pulse of the transmission signal [24]. However, this method is not efficient because it is difficult to generate the appropriate leakage signal amplitude. (3) Nonlinear schemes have been reported to filter out the second harmonic signal before feeding to the transducer [25]. The disadvantage of this scheme is that pre-definition of the inverted and mixed signals before obtaining the echo signal in the system level is necessary.

There is very little research that aims to improve performance of the high-voltage power amplifiers at the hardware level. A pre-linearizer scheme using look-up tables was developed to reduce harmonic distortion of the ultrasound echo signal [26]. However, the post-linearizer scheme was deemed to be more efficient because it can be physically connected to medical ultrasound transducers to enable direct control of the non-linear harmonic distortions generated by the transducers. Therefore, an HVPA incorporating a post-linearizer technique would facilitate the reduction of the harmonic effects of medical ultrasound transducers. To the best of our knowledge, this paper presents the first HVPA post-linearizer circuit technique for use in medical ultrasound transducers. The operating principles, design, and performance of the HVPA incorporating a post-linearizer will be described in this article.

One of the biggest challenges in HVPA design is achieving wide bandwidth and high linearity simultaneously. This is due to the parasitic impedances from electronic components, such as the power transistor, inductor and capacitor; and non-linear ultrasound transducers, including cable-loading effects [7,27]. Additionally, power transistor models are not accurately predictable at the circuit-design level [28,29]. Because most linearization techniques have been developed in narrow-band frequency ranges, it is thus quite difficult to design a linear broadband HVPA for used in medical ultrasound transducers [28]. Figure 1 is a drawing of the typical characteristics of the HVPA with and without the linearizer in medical ultrasound systems. The gain deviation curve of the HVPA should be flat for a wide range of input powers and frequencies because the HVPA must linearly amplify the signals with low signal distortion even at higher input power and frequency ranges.

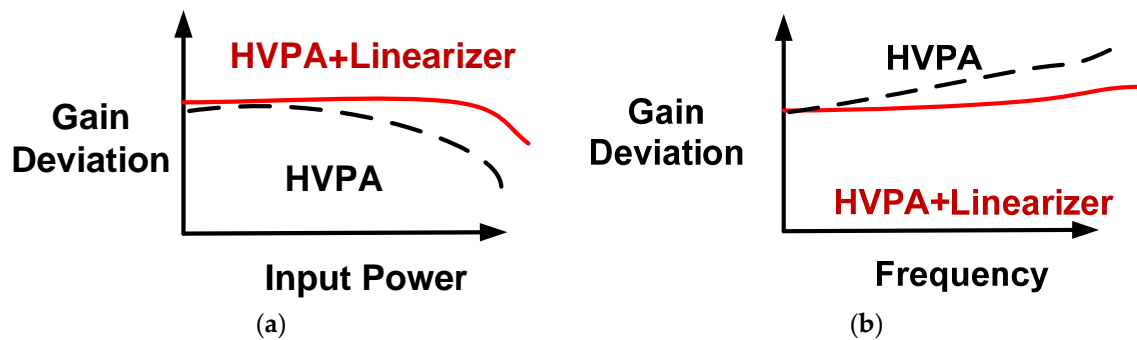


Figure 1. Gain deviation comparison between the high-voltage power amplifier (HVPA) with and without the linearizer as a function of (a) input power and (b) frequency (the black dashed lines and red solid lines represent the HVPA without and with the linearizer, respectively).

2. Materials and Methods

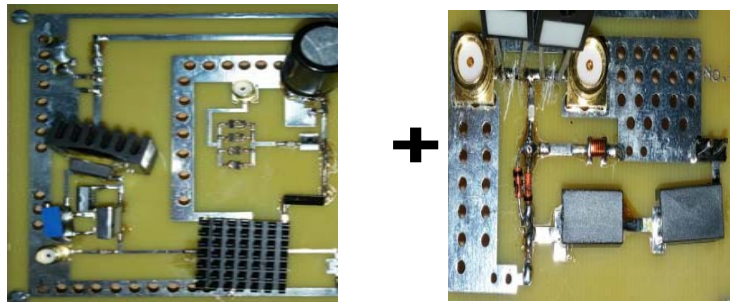
Figure 2a shows the Class-A type HVPA and post-linearizer. The circuits were implemented using discrete electronic components on a two-layer printed circuit board. As shown in Figure 2a, the HVPA is followed by the post-linearizer circuit.

In Figure 2b, 90 pF input and output DC coupling capacitors (C_{in} and C_{out} ; Vishay Intertechnology, Malvern, PA, USA) were placed at the input and output ports (“Input1” and “Output1”) to block the DC voltage and pass the AC signal. The simple resistor divider consists of a 2 k Ω variable resistor (R_{V1} ; Vishay Siliconix, Silver Lake Road, IL, USA) and 50 Ω fixed resistor (R_{V2} ; Caddock Electronics Inc., Riverside, CA, USA) with a high-voltage regulator (LM138; Texas Instrument, Austin, TX, USA) attached with a heat-sink (Aavid Thermalloy, San Jose, CA, USA). A 2 k Ω bias resistor (R_{B1} ; Caddock Electronics Inc., Riverside, CA, USA) and 3.5 μ H RF choke inductor (L_{ch2} ; Coilcraft Inc., Silver Lake Road, IL, USA) were used to block AC signal and minimize DC voltage drop. One 0.1 μ F electrostatic, two 1 μ F and 10 μ F capacitors (C_{DC1} , C_{DC2} , and C_{DC3} ; KEMET Corp., Simpsonville, CA, USA) were used to minimize the ripple current from the DC power supply (V_{DC} ; E3631A, Agilent Technology, Santa Clara, CA, USA). A 400 MHz 15 W RF MOSFET (M_{T1} ; PD57006-E, STMicroelectronics, Geneva, Switzerland) with heat-sink was used as the core transistor of the HVPA. Because of the high power output, separate heat sinks were utilized for the RF MOSFET and voltage regulator to prevent decrease of DC operating points in the RF MOSFET due to high temperature [30].

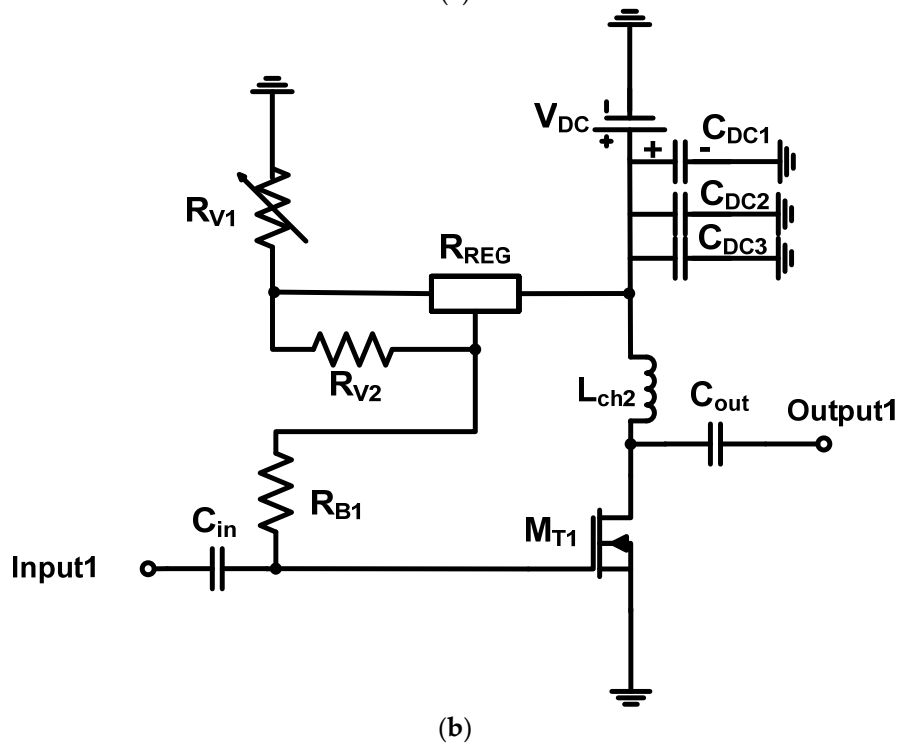
Our proposed post-linearizer circuit is presented in Figure 2c. All components of the HVPA and post-linearizer were high-voltage tolerant to prevent breakdown resulting from the single-cycle or multi-cycle high-voltage signals sent to the ultrasound transducer from the HVPA [14]. 30 pF capacitors (C_1 , C_2 , and C_{mid}), a 5.6 nH air-core high power inductor (L_1) and 5.1 nH high current inductors (L_2 and L_3) were also employed in the fabrication of the post-linearizer. The inductors (L_1 , L_2 , and L_3) were chosen to resonate with the corresponding capacitances (C_1 , C_2 , and C_{mid}) in the operating frequencies of the HVPA. Lastly, 50 W, 25 Ω power resistors (R_1 and R_2 ; Caddock Electronics), 0.5 cm and 1 cm transmission lines (TR_{in} and TR_{out}) and cross-coupled high speed switching diodes (DE_1 – DE_4 ; NXP semiconductors, Eindhoven, The Netherlands) were utilized to minimize ring-down artifact of the high-voltage bipolar pulse train signals that could reduce the ultrasound transducer bandwidth [10,31].

Figure 3 provides an equivalent HVPA circuit model of the HVPA to demonstrate the parasitic capacitances of the main transistor.

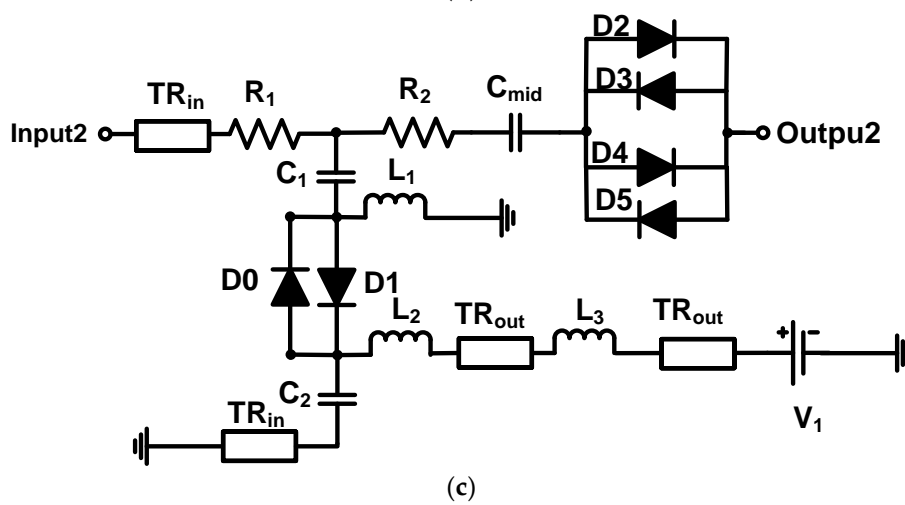
HVPA + Post-Linearizer



(a)



(b)



(c)

Figure 2. Block diagram and schematics of the HVPA and post-linearizer: (a) Implementation of the HVPA and post-linearizer, Schematics of the (b) HVPA, and (c) post-linearizer.

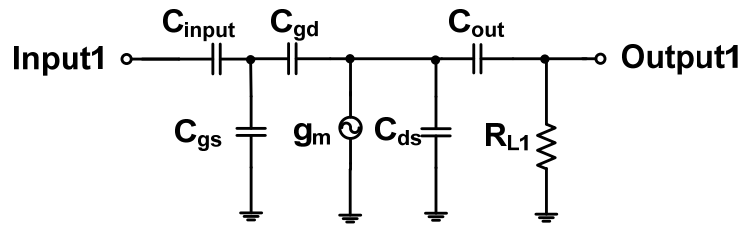


Figure 3. Equivalent circuit model of the HVPA.

The output of the HVPA can be expressed by

$$V_{out1} = -g_m \cdot V_{in1} \cdot \left\{ \frac{1}{j\omega C_i} // R_{L1} // \frac{1}{j\omega C_o} \right\} = \frac{-g_m \cdot V_{in1}}{\frac{1}{R_{L1}} + j\omega(C_i + C_o)} \quad (1)$$

where g_m is the transconductance of the transistor (M_{T1}), R_{L1} is the load resistance of the transistor (M_{T1}), and C_i is the combined input, parasitic gate-source, and gate-drain capacitances (C_{input} , C_{gs} and C_{gd}), and C_o is the combined drain-source and output capacitances of the transistor (C_{ds} and C_{out}).

As shown in Equation (1), the input and output capacitances of the transistor (C_i and C_o) could deteriorate HVPA performances. Therefore, the capacitance variation generated from the post-linearizer circuit was designed to compensate for the parasitic capacitances of the transistor. This is achieved by placing the input and output capacitance, in addition to the capacitances in the post-linearizer, in opposite positions in the Volterra series expansion [19,28,30]. Accordingly, non-linear compensation between the HVPA and post-linearizer was enhanced. A DC voltage (V_1) in the post-linearizer circuit was applied to offset the difference between the input capacitance variation of the transistor (M_{T1}) and the output impedance variation generated by the capacitors (C_1 and C_2), diodes ($D0$ – $D5$), and inductors (L_1 , L_2 , and L_3). Figure 4 illustrates the equivalent HVPA with post-linearizer circuit model used to analyze the non-linearity components. The large values of the bias inductor and RF choke inductors and small values of the transmission lines were eliminated in order to simplify the analysis.

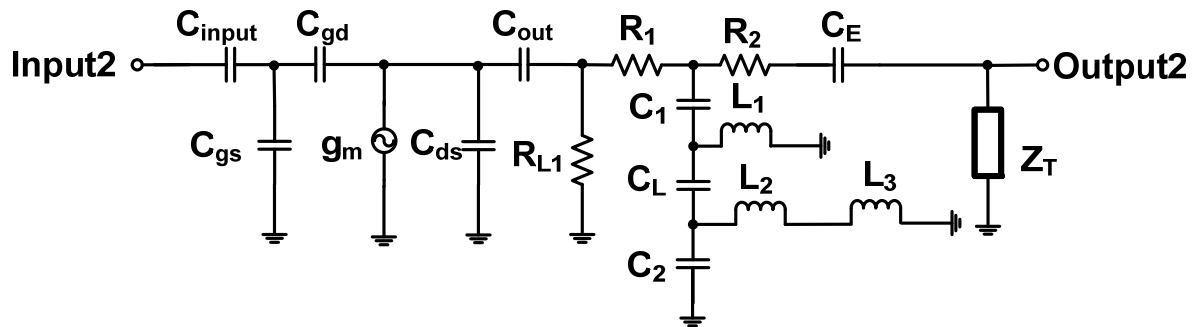


Figure 4. Equivalent circuit model of the HVPA with post-linearizer.

The total output of the HVPA with post-linearizer circuit (V_{out2}) with ultrasound transducer load can be expressed by

$$V_{out2} = -g_m \cdot V_{in1} \cdot \left\{ \frac{1}{j\omega(C_i + C_o)} + (R_{L1} // R_1) + \left(\frac{1}{j\omega C_2} // j\omega(L_1 + L_2) + \frac{1}{j\omega C_L} + \frac{1}{j\omega C_1} // j\omega L_1 \right) + (R_2 + \frac{1}{j\omega C_E}) // Z_T \right\} \quad (2)$$

$$\approx \frac{-g_m \cdot V_{in1}}{R_{L1} + R_1 + \left\{ \frac{1}{j\omega(C_i + C_o)} + \frac{1}{j\omega C_L} \right\} + \frac{1}{R_2 + j\omega C_E + Z_T}} Y_L = \frac{1}{j\omega C_2 + \frac{1}{j\omega L_{23}}} + j\omega C_L + \frac{1}{j\omega C_1 + \frac{1}{j\omega L_1}}$$

where C_1 and C_2 represent the equivalent capacitance of the capacitors C_1 and C_2 , C_L is the parasitic capacitance of the cross-coupled diode (D0 and D1), C_E is the total parasitic capacitances of the four switching diodes, and Z_T is the load impedance of the ultrasound transducer.

Equation (2) indicates that the parasitic capacitance variation of the input and output capacitances (C_i and C_o) with switching diodes and transducers could be compensated by the capacitors (C_1 and C_2) and diode equivalent capacitance (C_L) because, as previously mentioned, they yield opposite variations in large signal operations. Furthermore, the inductances in the post-linearizer (L_1 , L_2 and L_3) also compensate for these parasitic capacitances; thus, impedances resonate at the operating frequencies of the transducers. Therefore, non-linear characteristics of the HVPA with post-linearizer could be appropriately controlled over a wide range of input powers and frequencies. We expect that the 4 or 5 V DC voltage (V_1) in the post-linearizer circuit would be optimal to offset the non-linearity of the HVPA because, when using 25 V DC power supply voltage, the output junction (node connecting L_{ch2} and C_{out}) under approximately 20 V DC or AC voltage has a headroom of approximately 4–5 V DC voltage across the post-linearizer.

3. Results and Discussion

3.1. Experimental Performance Verification of the HVPA with Post-Linearizer

The impedance variation of the HVPA was found to be offset by the post-linearizer circuit, as described in the previous chapter. In order to verify this claim, the gain and gain deviation as a function of HVPA input power, and the frequency with and without the post-linearizer were measured, respectively. Figure 5 describes the measurement method. Input signals from an arbitrary function generator (AFG3252C, Tektronix Inc., Beaverton, OR, USA) were applied to the HVPA with or without the post-linearizer and DC power supply (E3631A, Agilent Technologies, Santa Clara, CA, USA). Subsequent to passing through the 20 dB power attenuator (BW-S20W20+, Mini-circuits, Brooklyn, NY, USA), the output waveform was measured in an oscilloscope (MSOX4154A, Keysight Technology, Santa Clara, CA, USA). A power attenuator was used to reduce the high-voltage when measuring the results, as the maximum voltage was restricted to 5 V in the 50 Ω input impedance setting of the oscilloscope.

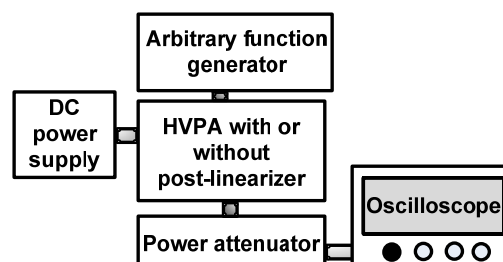


Figure 5. Measurement setup to calculate the gain as a function of HVPA input power and frequency with and without the post-linearizer.

Figure 6a–d illustrates that the measured gain and gain deviation of the HVPA with and without the post-linearizer, respectively. 10 MHz, 5-cycle input power signals were applied to the HVPA when 1, 2, 4, and 5 V DC voltages were applied to the post-linearizer. The output signals were then measured in order to calculate the gain and gain deviation of the HVPA with and without the post-linearizer. The input 1 dB compression point (IP_{1dB}) defines the limited linearity index of the power amplifier, which is the point at which the amplifier gain is 1 dB below the initial gain [30,32]. Thus, the IP_{1dB} of the HVPA with and without post-linearizer were measured and compared in order to evaluate the linearity of the HVPA without and with post-linearizer, respectively.

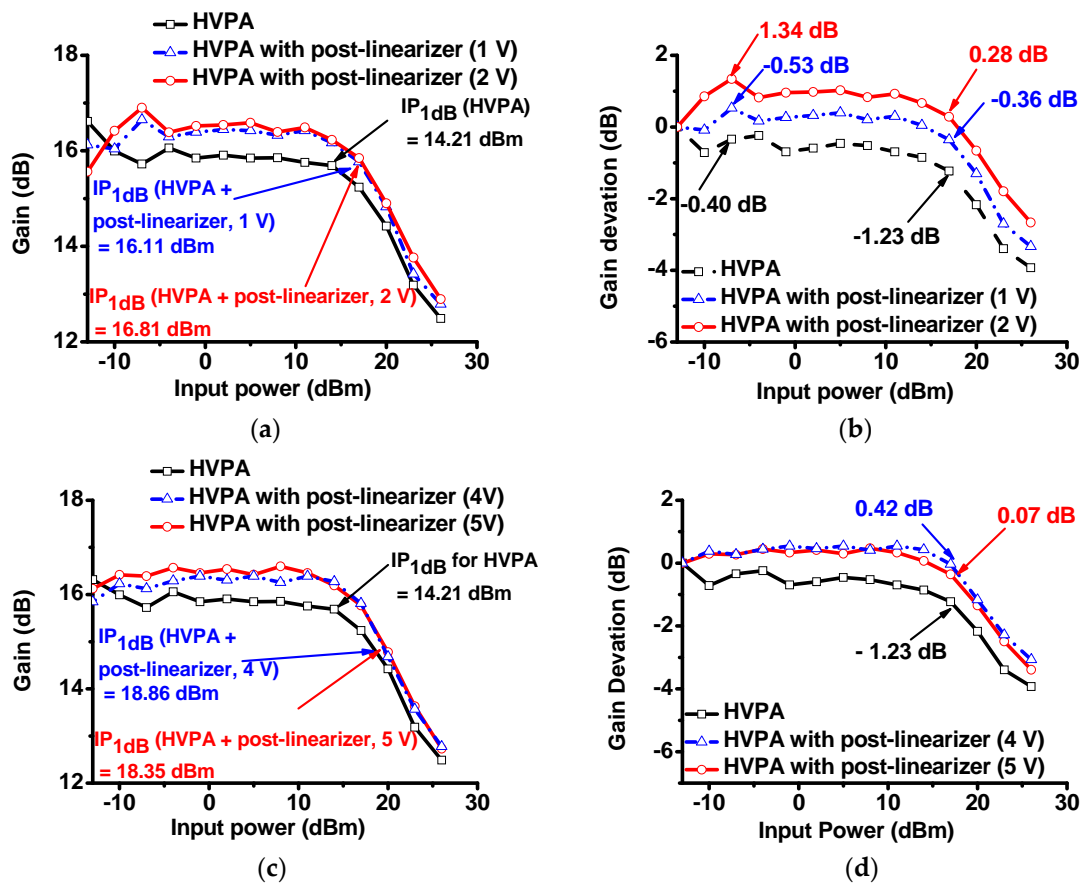


Figure 6. (a) Gain and (b) gain deviation vs. input power of the HVPA without the post-linearizer (solid black lines) and HVPA with post-linearizer with 1 V and 2 V DC applied voltages (solid red lines and dash-dot blue lines, respectively); (c) Gain and (d) gain deviation vs. input power of the HVPA without the post-linearizer (solid black lines) and HVPA with post-linearizer with 4 and 5 V DC voltage applied (solid red lines and dash-dot blue lines, respectively).

As shown in Figure 6a, the gain of the HVPA with post-linearizer when 1 V and 2 V DC voltage were applied to the post-linearizer increased to -4 dB_m, and then decreased to -1 dB_m input power. However, the IP_{1dB} of the HVPA (14.21 dB_m) was lower than that for the HVPA with post-linearizer when 1 and 2 V DC voltage were applied (16.11 dB_m and 16.81 dB_m, respectively). As shown in Figure 6b, the gain deviation of the HVPA, and that of the HVPA with post-linearizer when 1 V and 2 V DC voltages were applied, yielded instability up to approximately -1 dB_m input power. The gain deviation of the HVPA (-0.40 dB at -4 dB_m input power) was lower than that of the HVPA when 1 V and 2 V DC voltages were applied to the post-linearizer (-0.53 dB and 1.34 dB at -4 dB_m input power, respectively). However, the gain deviation of the HVPA with the post-linearizer when 1 V and 2 V DC voltages were applied (-0.36 dB and 0.28 dB at 17 dB_m) was lower than that of the HVPA without post-linearizer (-1.23 dB at 17 dB_m). The gain of the HVPA with post-linearizer yielded moderate stability between -1 dB_m and 26 dB_m when 1 V and 2 V DC voltages were applied to the post-linearizer. These results confirm that, for 1 V and 2 V DC voltage, a minimum input power of -4 dB_m is required to obtain efficient operation of the post-linearizer.

Figure 6c,d shows the measured gain and gain deviation of the HVPA with and without linearizer, respectively. As shown in Figure 6c, the overall trend of gain of the HVPA with post-linearizer for the cases of 4 V and 5 V DC applied voltages is flatter than that of the HVPA without post-linearity. This is due to the IP_{1dB} for the HVPA (14.21 dB_m) being substantially lower than that for the HVPA with post-linearizer when 4 V and 5 V DC voltages were applied (18.86 dB_m and 18.35 dB_m, respectively).

In accordance with the results from circuit design analysis (Equations (1) and (2)), the post-linearizer exhibited adequate capacity to operate efficiently over a wide input-power range when 4 V and 5 V DC voltages were applied. In Figure 6d, the gain deviation of the HVPA with post-linearizer when 4 V and 5 V DC voltages were applied (0.42 dB and 0.07 dB at 17 dB_m input power, respectively) was lower than that of the HVPA without the linearizer (−1.23 dB at 17 dB_m). When 4 V and 5 V DC voltages were applied to the post-linearizer, the change in gain deviation of the HVPA with post-linearizer was from less than approximately 1 dB up to approximately 20 dB_m input power. Additionally, the gain deviation values of the HVPA with post-linearizer were less than those of the HVPA without the post-linearizer up to 26 dB_m input power. As also derived in Equation (2), we can conclude that the post-linearizer improves gain stability of the HVPA over a wide input power range because the post-linearizer circuit can offset the non-linearity of the input capacitances of transistor devices.

Figure 7 illustrates the measured output power versus the input power when 10 MHz, 10-, 15-, 20-, 25-cycle pulse signals were applied to the HVPA with the post-linearizer in order to test for IP_{1dB} variances associated with higher input pulsed power. As shown in Figure 7, analysis of IP_{1dB} as a function of input power of the HVPA with post-linearizer when 1 V DC voltage was applied yielded the following results: 16.13 dB_m, 16.17 dB_m, 16.22 dB_m, and 16.19 dB_m, respectively. Analysis of IP_{1dB} as a function of input power of the HVPA with post-linearizer when 2 V DC voltage was applied yielded the following results: 16.50 dB_m, 16.71 dB_m, 16.71 dB_m, and 16.75 dB_m, respectively. Additionally, IP_{1dB} as a function of input power of the HVPA with post-linearizer when 4 V DC voltage was applied yielded the following results: 17.42 dB_m, 17.32 dB_m, 17.63 dB_m, and 17.69 dB_m, respectively. Lastly, analysis of IP_{1dB} as a function of input power of the HVPA with post-linearizer when 5 V DC voltage was applied yielded the following results: 18.31 dB_m, 18.16 dB_m, 18.23 dB_m, and 18.28 dB_m, respectively. The measured variances of the IP_{1dB} of the HVPA with the post-linearizer were less than 0.5 dB_m, representing considerably low variances. Measured IP_{1dB} values of the HVPA with the post-linearizer under 1 V, 2 V, 3 V, 4 V and 5 V DC voltages were higher than that of the HVPA without the post-linearizer. Moreover, the measured IP_{1dB} values of the HVPA with the post-linearizer under 4 V and 5 V DC voltages were higher than that of the HVPA without the post-linearizer when the same DC voltages were applied. From this analysis, we can confirm that the IP_{1dB} of the HVPA with post-linearizer under higher DC voltages (4 V and 5 V) continued to yield improved efficiency compared to the HVPA without the post-linearizer.

Figure 8 shows the measured gain and gain deviation as a function of frequency of the HVPA with and without the post-linearizer, respectively because the harmonic technique may be implemented with the 10 MHz ultrasonic transducer. The setup to measure the gain as a function of frequency is identical to that depicted in Figure 5. A fixed 17 dBm input power from the arbitrary function generator (AFG3252C) was applied to the HVPA and the HVPA with post-linearizer to measure the output voltages via the oscilloscope (MSOX4154A) and subsequently, the gain and gain deviation of the devices were calculated. In Figure 8a, the measured gains of the HVPA with and without post-linearizer are 15.6 and 15.2 dB at 10 MHz, and 16.5 and 11.1 dB at 40 MHz, respectively. Thus, we confirm from these results that the gain of the HVPA with post-linearizer exhibited greater flatness than that of the HVPA without the post-linearizer. In Figure 8b, the gain deviation values were calculated based on how much the gain at each frequency (6 MHz to 40 MHz) deviated from the measured gain at 10 MHz frequency. The gain deviation of the HVPA with post-linearizer yielded values smaller than that of the HVPA without the post-linearizer throughout the mid-range frequencies, but was higher than that of HVPA without the post-linearizer at the highest measured frequency (with post-linearizer: 1.01 dB and 0.90 dB at 26 MHz and 40 MHz, respectively, and without the post-linearizer: 1.60 dB and −3.12 dB at 26 MHz and 40 MHz, respectively). These measured results are significant because the operating frequency of the ultrasound transducer could vary depending on the cable effect and electrical impedances of the systems [7]. Therefore, an ultrasound transmitter such as the HVPA, which yields adequate operation over a wide bandwidth, is preferred for integration with ultrasound transducers.

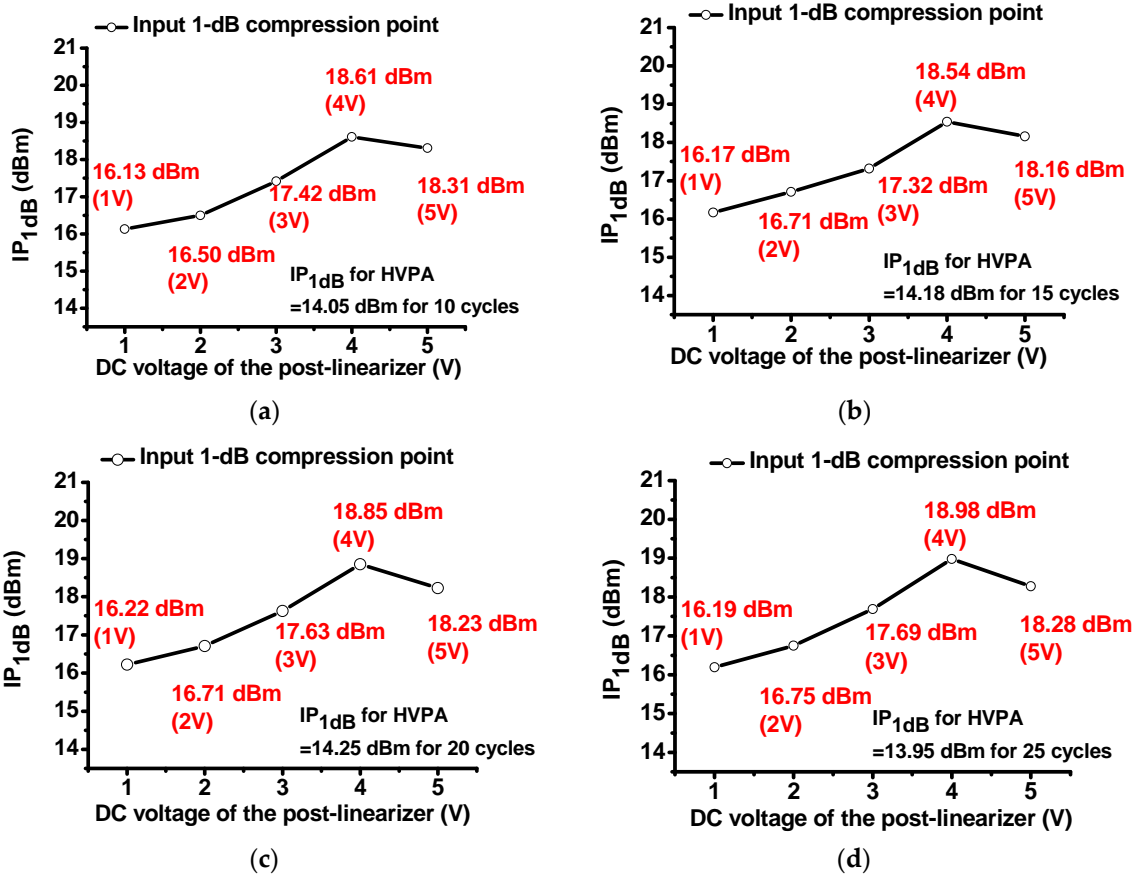


Figure 7. Output power vs. input power of the HVPA without the post-linearizer (value provided in each figure) and HVPA with post-linearizer (solid black lines) with 10 MHz, (a) 10-, (b) 15-, (c) 20-, and (d) 25-cycle pulse signals sent to the HVPA with and without the post-linearizer, respectively.

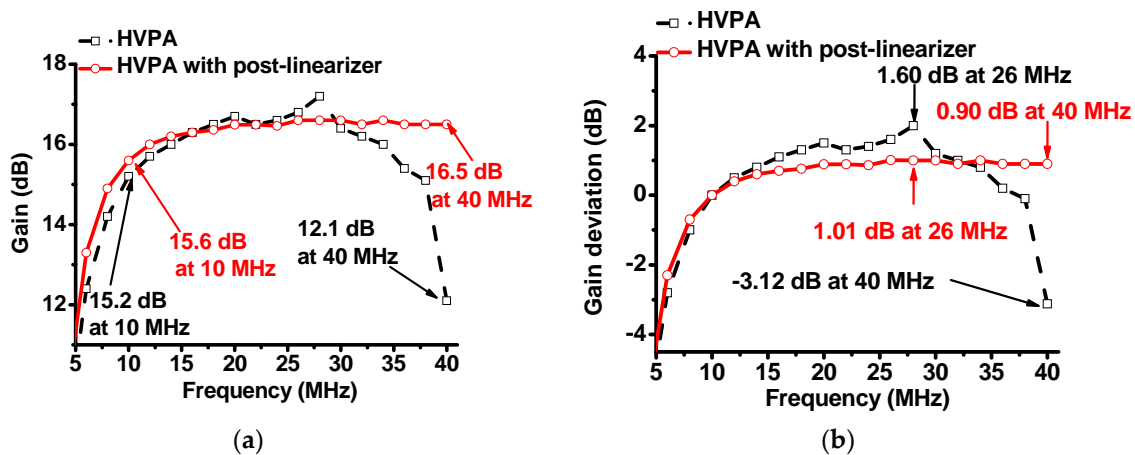


Figure 8. (a) Gain vs. frequency and (b) gain deviation vs. frequency of the HVPA without the post-linearizer (black-dashed line) and HVPA with post-linearizer when 17 dB_m input power was applied.

3.2. Performance of the Pulse-Echo Response of the Ultrasound Bio-Microscopy (UBM) System

Linearizing the HVPA could reduce harmonic distortion of the HVPA itself [19]. The HVPA stimulates the generation of the ultrasound waves by the transducer. Thus, linearizing the HVPA can suppress the harmonic distortion components of the ultrasound transducer, thereby improving the echo signal quality of the ultrasound system.

Figure 9a presents the design of a proposed ultrasound biomicroscopy (UBM) system using an HVPA with and without the post-linearizer. The UBM system is useful for estimating ultrasound transducer and ultrasound system performance because newly-developed transducers or electronic components need to be tested before integration in ultrasound systems [33]. In this study, the input power signal was sent to the HVPA with and without the post-linearizer in order to activate the 10 MHz immersion ultrasound transducer (V311-SU, Olympus NDT, Inc., Waltham, MA, USA). The detected echo signal produced by the transducer passed through the protection circuit composed of a 50 Ω power resistor (Caddock Electronics Inc.) shunt with a single crossed-diode pair (NXP Semiconductors) and was subsequently amplified by the 40 dB voltage gain preamplifier (AU-1114, MITEQ Inc., Hauppauge, NY, USA). The echo signal was displayed on the oscilloscope (MSOX4154A) in order to process the spectrum data on a personal computer.

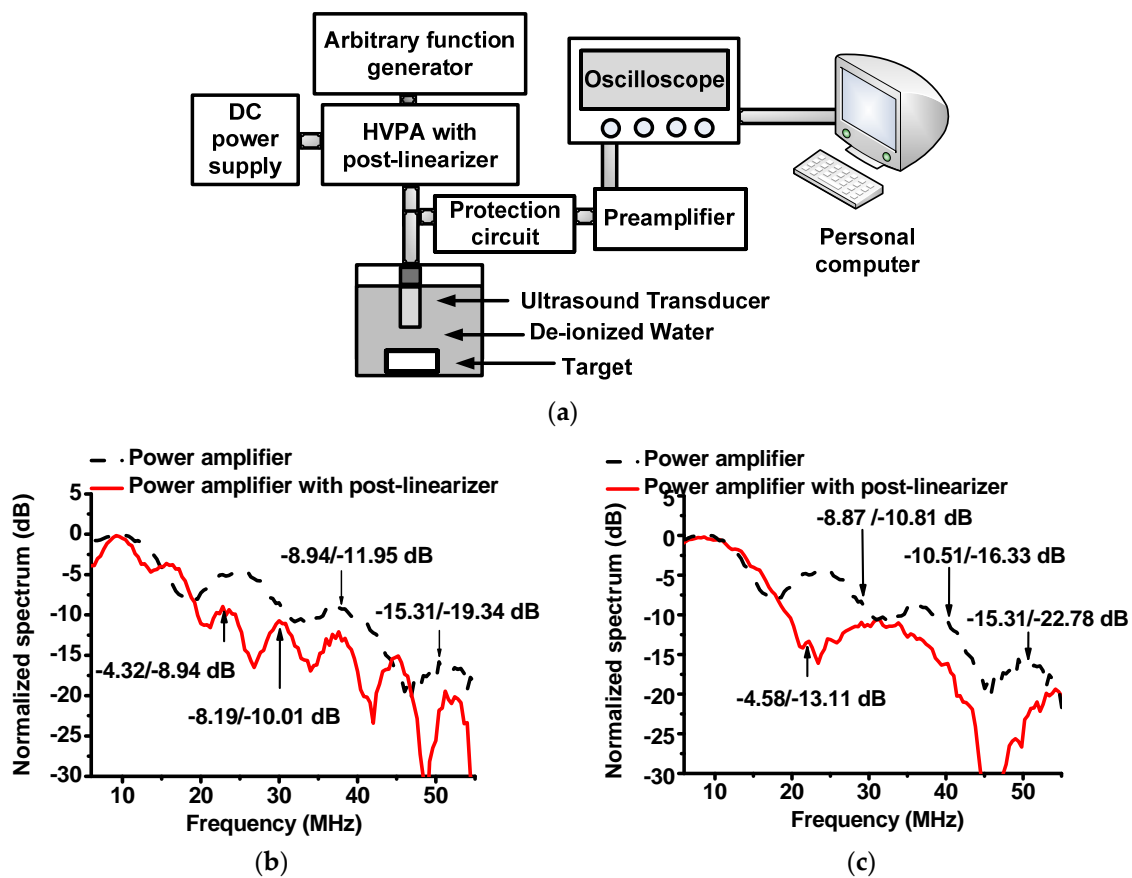


Figure 9. Block diagram of the UBM system and spectrum data of the echo signal generated by a 10 MHz ultrasound transducer with and without post-linearizer circuit: (a) Block diagram of the UBM system; (b) 10 MHz, 20-cycle and 17 dB_m input power, and 4 V DC voltage applied to the HVPA with and without post-linearizer; (c) 10 MHz, 5-cycle and 26 dB_m input power, and 4 V DC voltage applied to the HVPA with and without post-linearizer.

Figure 9b,c illustrates the measured normalized spectrum as a function of the echo signal frequency generated by a 10 MHz ultrasound transducer for the HVPA with and without the post-linearizer circuit, respectively. As shown in Figure 9b, a 10 MHz, 20-cycle, 17 dB_m input power sinewave pulsed signal was applied to the HVPA, and 4 V DC voltage was applied to the linearizer. With 17 dB_m input, the second-, third-, fourth- and fifth-harmonic distortion components of the echo signal of the HVPA with post-linearizer (−8.94 dB, −10.01 dB, −11.95 dB, and −19.34 dB) were lower than those of the echo signal of HVPA without the post-linearizer (−4.32 dB, −8.19 dB, −8.94 dB, and −15.31 dB),

respectively. As shown in Figure 9c, a 10 MHz, 5-cycle 26 dB_m input power sinewave burst signal was applied to the HVPA and 4 V DC voltage was applied to the post-linearizer. With a 26 dB_m input, the second-, third-, fourth- and fifth-harmonic distortion components of the echo signal of HVPA with post-linearizer (−13.11 dB, −11.8 dB, −16.33 dB and −22.78 dB) were lower than those of the echo signal of HVPA without the post-linearizer (−4.58 dB, −8.87 dB, −10.51 dB and −15.31 dB), respectively. As shown in Figure 9b,c, harmonic signal components of the HVPA with post-linearizer were suppressed more than those of HVPA without post-linearizer. Therefore, we conclude that the post-linearizer circuit can suppress various undesirable harmonic distortion components of the ultrasound transducer-generated echo signal.

4. Conclusions

In ultrasound techniques such as harmonic techniques and the coded excitation method, low-harmonic distortion components of the echo signal from ultrasound transducers are desired to obtain high-quality echo signal in ultrasound systems. A linear HVPA is preferable because it can suppress non-linear harmonic distortion components of ultrasound echo signals. To the best of our knowledge, this paper presents the first post-linearizer circuit to linearize the HVPA gain over a broad bandwidth. Results demonstrated that the capacitances in the post-linearizer nullified the parasitic input capacitances of the transistor, and inductances of the post-linearizer were able to resonate with the input and output and capacitances of the transistor, resulting in a reduction of the harmonic distortion components of the echo signal that lead to the development of an efficient HVPA that yielded adequate wide-bandwidth operation. The post-linearizer technique introduced here may be effective in precisely suppressing the non-linearity of ultrasound transducer.

Lower second-, third-, fourth- and fifth-harmonic distortion components of the echo signal (−8.94 dB, −10.01 dB, −11.95 dB, and −19.34 dB) were attained by the HVPA with post-linearizer circuit in UBM systems as compared to those of the HVPA without post-linearizer (−4.32 dB, −8.19 dB, −8.94 dB, and −15.31 dB). Considering these results, the proposed post-linearizer circuit demonstrated potential to be used as a method to achieve gain performance linearization of the HVPA over a wide range of input powers and frequencies.

Acknowledgments: This work has been supported by National Research Foundation of Korea (NRF-2016M2B2 A9A02945226) and by the MSIP (Ministry of Science, ICT and Future Planning), Korea, under the ITRC (Information Technology Research Center) support program (IITP-2016-R2718-16-0015) supervised by the IITP (National It Industry Promotion Agency).

Author Contributions: C. Yoon and H. Choi conceived the idea, J. Y. Yeom and H. Choi carried out the experiments; J.Y. Yeom, C. Yoon and H. Choi analyzed the data and wrote the paper together.

Conflicts of Interest: The authors declare no conflict of interest.

References

1. Lee, J.; Shung, K.K. Radiation forces exerted on arbitrarily located sphere by acoustic tweezer. *J. Acoust. Soc. Am.* **2006**, *120*, 1084–1094. [[CrossRef](#)] [[PubMed](#)]
2. Blitz, J.; Simpson, G. *Ultrasonic Methods of Non-Destructive Testing*; Springer: Berlin, Germany, 1995; Volume 2.
3. Lee, S.-H.; Jeong, H.-H.; Bae, S.-B.; Choi, H.-C.; Lee, J.-H.; Lee, Y.-H. Epitaxially grown gan thin-film saw filter with high velocity and low insertion loss. *IEEE Trans. Electron. Devices* **2001**, *48*, 524–529.
4. Ritter, T.A.; Shrout, T.R.; Tutwiler, R.; Shung, K.K. A 30-MHz piezo-composite ultrasound array for medical imaging applications. *IEEE Trans. Ultrason. Ferroelectr. Freq. Control* **2002**, *49*, 217–230. [[CrossRef](#)] [[PubMed](#)]
5. Zhu, X.; Guo, J.; He, C.; Geng, H.; Yu, G.; Li, J.; Zheng, H.; Ji, X.; Yan, F. Ultrasound triggered image-guided drug delivery to inhibit vascular reconstruction via paclitaxel-loaded microbubbles. *Sci. Rep.* **2016**, *6*, 21683. [[CrossRef](#)] [[PubMed](#)]
6. Hoskins, P.R.; Martin, K.; Thrush, A. *Diagnostic Ultrasound: Physics and Equipment*; Cambridge University Press: Cambridge, UK, 2010.
7. Szabo, T.L. *Diagnostic Ultrasound Imaging: Inside Out*; Elsevier Academic Press: London, UK, 2004.

8. Zhu, B.; Chan, N.Y.; Dai, J.; Shung, K.K.; Takeuchi, S.; Zhou, Q. New fabrication of high-frequency (100-MHz) ultrasound PZT film kerfless linear array. *IEEE Trans. Ultrason. Ferroelectr. Freq. Control* **2013**, *60*, 854–857. [[CrossRef](#)] [[PubMed](#)]
9. Kirk Shung, K.; Smith, M.B.; Tusi, B.M.W. *Principles of Medical Imaging*; Academic Press, Inc.: San Diego, CA, USA, 1992.
10. Shung, K.K. *Diagnostic Ultrasound: Imaging and Blood Flow Measurements*; Taylor & Francis: Boca Raton, FL, USA, 2015.
11. Ketterling, J.A.; Aristizabal, O.; Turnbull, D.H.; Lizzi, F.L. Design and fabrication of a 40-MHz annular array transducer. *IEEE Trans. Ultrason. Ferroelectr. Freq. Control* **2005**, *52*, 672–681. [[CrossRef](#)] [[PubMed](#)]
12. He, Z.; Zheng, F.; Ma, Y.; Kim, H.H.; Zhou, Q.; Shung, K.K. A sidelobe suppressing near-field beamforming approach for ultrasound array imaging. *J. Acoust. Soc. Am.* **2015**, *137*, 2785–2790. [[CrossRef](#)] [[PubMed](#)]
13. Zhou, Q.; Lau, S.; Wu, D.; Shung, K.K. Piezoelectric films for high frequency ultrasonic transducers in biomedical applications. *Prog. Mater. Sci.* **2011**, *56*, 139–174. [[CrossRef](#)] [[PubMed](#)]
14. Shung, K.K.; Zippuro, M. Ultrasonic transducers and arrays. *IEEE Eng. Med. Biol. Mag.* **1996**, *15*, 20–30. [[CrossRef](#)]
15. Tranquart, F.; Grenier, N.; Eder, V.; Pourcelot, L. Clinical use of ultrasound tissue harmonic imaging. *Ultrasound Med. Biol.* **1999**, *25*, 889–894. [[CrossRef](#)]
16. Choudhry, S.; Gorman, B.; Charboneau, J.W.; Tradup, D.J.; Beck, R.J.; Kofler, J.M.; Groth, D.S. Comparison of tissue harmonic imaging with conventional US in abdominal disease 1. *Radiographics* **2000**, *20*, 1127–1135. [[CrossRef](#)] [[PubMed](#)]
17. Pasovic, M.; Danilouchkine, M.; Matte, G.; van der Steen, A.F.; Basset, O.; de Jong, N.; Cachard, C. Broadband reduction of the second harmonic distortion during nonlinear ultrasound wave propagation. *Ultrasound Med. Biol.* **2010**, *36*, 1568–1580. [[CrossRef](#)] [[PubMed](#)]
18. Song, J.; Kim, S.; Sohn, H.-Y.; Song, T.-K.; Yoo, Y.M. Coded excitation for ultrasound tissue harmonic imaging. *Ultrasonics* **2010**, *50*, 613–619. [[CrossRef](#)] [[PubMed](#)]
19. Katz, A. Linearization: Reducing distortion in power amplifiers. *IEEE Microw. Mag.* **2001**, *2*, 37–49. [[CrossRef](#)]
20. Aparin, V. Linearization of CDMA Receiver Front-Ends. Ph.D. Dissertation, University of California, San Diego, CA, USA, 2005.
21. Zwiebel, W.J.; Pellerito, J.S. *Introduction to Vascular Ultrasonography*; Elsevier Saunders Philadelphia: Philadelphia, PA, USA, 2005.
22. Kirkhorn, J.; Frinking, P.J.; de Jong, N.; Torp, H. Three-stage approach to ultrasound contrast detection. *IEEE Trans. Ultrason. Ferroelectr. Freq. Control* **2001**, *48*, 1013–1022. [[CrossRef](#)] [[PubMed](#)]
23. Simpson, D.H.; Chin, C.T.; Burns, P.N. Pulse inversion doppler: A new method for detecting nonlinear echoes from microbubble contrast agents. *IEEE Trans. Ultrason. Ferroelectr. Freq. Control* **1999**, *46*, 372–382. [[CrossRef](#)] [[PubMed](#)]
24. Shen, C.-C.; Li, P.-C. Pulse-inversion-based fundamental imaging for contrast detection. *IEEE Trans. Ultrason. Ferroelectr. Freq. Control* **2003**, *50*, 1124–1133. [[CrossRef](#)] [[PubMed](#)]
25. Krishnan, S.; Hamilton, J.D.; O'Donnell, M. Suppression of propagating second harmonic in ultrasound contrast imaging. *IEEE Trans. Ultrason. Ferroelectr. Freq. Control* **1998**, *45*, 704–711. [[CrossRef](#)] [[PubMed](#)]
26. Gao, Z.; Gui, P. A look-up-table digital predistortion technique for high-voltage power amplifiers in ultrasonic applications. *IEEE Trans. Ultrason. Ferroelectr. Freq. Control* **2012**, *59*. [[CrossRef](#)]
27. Cannata, J.M.; Williams, J.A.; Zhou, Q.; Ritter, T.A.; Shung, K.K. Development of a 35-MHz piezo-composite ultrasound array for medical imaging. *IEEE Trans. Ultrason. Ferroelectr. Freq. Control* **2006**, *53*, 224–236. [[CrossRef](#)] [[PubMed](#)]
28. Vuolevi, J.; Rahkonen, T. *Distortion in RF Power Amplifiers*; Artech House: London, UK, 2003.
29. Lee, T.H. *The Design of CMOS Radio-Frequency Integrated Circuits*; Cambridge University Press: Cambridge, UK, 2004.
30. Cripps, S.C. *Advanced Techniques in RF Power Amplifier Design*; Artech House: London, UK, 2002.
31. Gundersen, M.; Kuthi, A.; Behrend, M.; Vernier, T. Bipolar Nanosecond Pulse Generation Using Transmission Lines for Cell Electro-Manipulation. In Proceedings of IEEE Power Modulator Symposium, San Francisco, CA, USA, 23–26 May 2004; pp. 224–227.

32. Kazimierczuk, M.K. *RF Power Amplifier*; John Wiley & Sons: Hoboken, NJ, USA, 2014.
33. Zhu, B.; Han, J.; Shi, J.; Shung, K.K.; Wei, Q.; Huang, Y.; Kosec, M.; Zhou, Q. Lift-off pmn-pt thick film for high frequency ultrasonic biomicroscopy. *J. Am. Ceram. Soc. Am. Ceram. Soc.* **2010**, *93*, 2929–2931. [[CrossRef](#)] [[PubMed](#)]



© 2017 by the authors. Licensee MDPI, Basel, Switzerland. This article is an open access article distributed under the terms and conditions of the Creative Commons Attribution (CC BY) license (<http://creativecommons.org/licenses/by/4.0/>).